Modelling the creep rates of eutectic Bi–Sn solder using the data from its constitutive phases

C. H. RAEDER
Advanced Micro Devices, Austin, TX, USA

D. MITLIN
Department of Materials Science, University of California, Berkeley, and Lawrence Berkeley National Laboratory, Berkeley, CA 94720, USA

R. W. MESSLER, Jr
Department of Materials Science and Engineering at Rensselaer Polytechnic Institute, Troy, NY, USA
E-mail: mitlin@uclink4.berkeley.edu

Constitutive equations obtained from the creep behaviour of 99.9 wt % pure Bi and from Sn–10 wt % Bi single-phase solid solution are applied in the continuum mechanics creep model of Tanaka et al. [1] to predict the creep behaviour of a eutectic Bi–42 wt % Sn alloy. At low stresses, Bi is the load bearing phase, while at high stresses, Sn–10 wt % Bi is the load bearing phase. The continuum mechanics creep model is able to predict the shape of the steady-state versus strain curves. However, the model predicts creep rates that are generally lower than the data. This inconsistency may be caused by a phase boundary sliding contribution to the creep rate, which is unaccounted for by the model. Creep tests done on Sn–42 wt % Bi samples having various microstructural morphologies support this conclusion, where the more spheroidized microstructure creeps faster. © *1998 Kluwer Academic Publishers*

1. Introduction

Low melting temperature (139 °C) eutectic Bi–42 wt % Sn alloy is becoming an increasingly attractive soldering alloy for the growing number of temperature-sensitive electronic assemblies where conventional eutectic Sn–Pb solder (melting temperature of 183 °C) cannot be used. As with all solders, creep during service is a major concern for Bi–42 wt % Sn because it operates at such high homologous temperatures (typically between room temperature and 125 °C).

Previous studies [2, 3] have demonstrated the existence of three regions of different stress dependence in the steady-state creep regime. A representative selection of the Bi–42 wt % Sn steady-state creep data taken at 60 °C is shown in Fig. 1 [2, 3]. At stresses below 5 MPa, the stress exponent is near five. At intermediate stresses, $3 > \sigma > 20$ MPa, the stress exponent is approximately three. Above 20 MPa the stress exponent is not constant, but increases with stress (it is five or higher). For a single-phase alloy, these three regions can be attributed to the following rate limiting mechanisms. A stress exponent of five is associated with annihilation of edge dislocations through climb [4, 5]. A stress exponent of three corresponds to dislocation glide through solute atmospheres [6]. A stress exponent greater than five can correspond to creep controlled by dislocation climb occurring by pipe diffusion [7]; creep under conditions of an active dislocation density, which is inversely proportional to stress [8]; or creep under powerlaw breakdown [9]. A series of creep mechanisms, similar to what is described above, has been observed in Al–5.6 at. % Mg [10]. However, unlike single-phase Al–5.6 at. % Mg, Bi–42 wt % Sn is a two-phase composite. It is composed of nearly equal volume fractions of a Bi phase with a negligible solubility of Sn, and a Sn-rich phase with a maximum solubility of 21 wt % Bi at the eutectic temperature. Therefore, before ascribing any particular creep mechanism to a certain stress regime, one must first know the creep behaviour of the separate phases and their interactions in the composite.

Deformation behaviour of two-phase materials is described by numerous authors [1, 11–17]. Their individual approaches vary widely, from the use of the mechanical law of mixtures [11–14], to finite element methods [15], to continuum mechanics models [1, 16, 17]. The model of Tanaka et al. [1] is examined in this work because it has been demonstrated to be effective in predicting specifically the creep response of two-phase composites [1], whereas the other models tend to be more general. In this paper, their model will be referred to as the continuum mechanics composite creep (CMCC) model.

The CMCC model assumes both phases are elastically and plastically isotropic and that creep strains
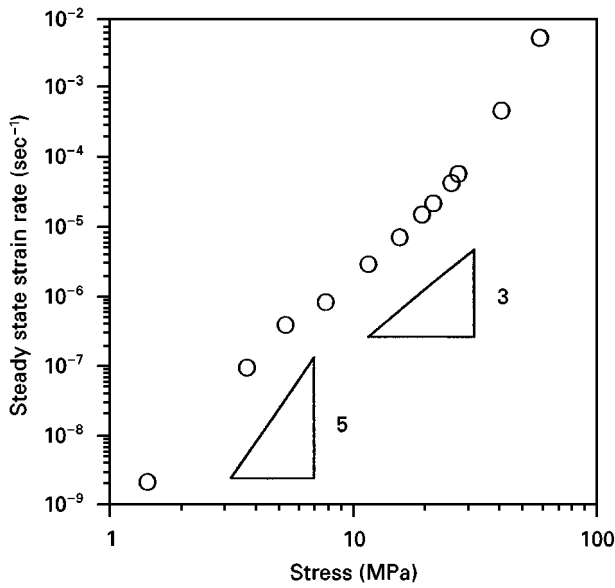
Figure 1 Creep of Bi–42 wt % Sn showing sigmoidal stress dependence (○ 333 K).

are uniform in the individual phases, namely $\varepsilon_{33}^{I} = -2\varepsilon_{11}^{I} = -2\varepsilon_{22}^{I}$ for the matrix (phase I) and $\varepsilon_{33}^{II} = -2\varepsilon_{11}^{II} = -2\varepsilon_{22}^{II}$ for the second phase (phase II) under an applied tensile stress, σ_{33}^{A} [1]. Internal stresses exist due to the strain differences, $\Delta\varepsilon_{11} = \varepsilon_{11}^{I} - \varepsilon_{11}^{II}$, $\Delta\varepsilon_{22} = \varepsilon_{22}^{I} - \varepsilon_{22}^{II}$, and $\Delta\varepsilon_{33} = \varepsilon_{33}^{I} - \varepsilon_{33}^{II}$, arising during the early stages of creep. The components of internal stress averaged over the matrix, σ_{ij}^{I}, and second phase, σ_{ij}^{II}, are calculated by Eshelby's equivalent inclusion method [18, 19] and Mori–Tanaka's average internal stress concept [20] and are expressed as

$$\sigma_{33}^{I} = fAE\Delta\varepsilon_{33} = -fAEx$$
$$\sigma_{11}^{I} = \sigma_{22}^{I} = fBE\Delta\varepsilon_{33} = fBEx$$
$$\sigma_{33}^{II} = (1-f)AEx \qquad (1)$$
$$\sigma_{11}^{II} = \sigma_{22}^{II} = -(1-f)BEx$$

where f is the volume fraction of the second phase, x is the phase strain difference ($x = \Delta\varepsilon_{33}$), E is Young's modulus for the two-phase alloy, and A and B are functions of Eshelby's tensor and of the elastic moduli of the matrix and second phase [21–23]. The actual stresses acting on the matrix phase are then given by

$$\sigma_{33}^{A} + \sigma_{33}^{I} = \sigma_{33}^{A} - fAEx$$
$$\sigma_{22}^{I} = \sigma_{11}^{I} = fBEx \qquad (2)$$

The stresses in the second phase are similarly defined. These triaxial stresses, through the von Mises relation, are expressed as equivalent stresses, σ_{e}^{i}, which, following simplification, are given by

$$\sigma_{e}^{I} = \sigma_{33}^{A} - fKEx$$
$$\sigma_{e}^{II} = \sigma_{33}^{A} - (1-f)KEx \qquad (3)$$

where $K (= A + B)$ is termed the shape factor, and is generally between 0.5 and 1.5 [1].

A numerical simulation (done in Visual Basic) is used to calculate the strain versus time response of the two-phase alloy. First, the two-phase sample is loaded to the specified stress. The equivalent stresses (initially equal to σ_{33}^{A}) are used in the unidirectional creep laws for the individual phases. The calculated creep rates are then multiplied by the time increment (in the numerical simulation) to get the creep strains of the individual phases. The creep strain of the alloy is given by

$$\varepsilon_{33} = (1-f)\varepsilon_{33}^{I} + f\varepsilon_{33}^{II} \qquad (4)$$

The phase strain difference is summed with the previous difference, the stress distribution is modified, the phase creep rates are again calculated, and so on in an iterative fashion to construct the complete strain–time response. Steady-state creep is attained when the creep rates in each phase are equal.

The goal of this study is to illustrate, using the CMCC model, how both the pure Bi phase and Sn–10 wt % Bi contribute to the creep of the eutectic alloy. In the past, this model has been successfully used to predict creep in ferrite–pearlite steels and in Cu–W wires [1]. Both microstructures consisted of geometrically well defined phases; W wires uniformly embedded in a Cu matrix, while the ferrite–pearlite steels had the major phase (either one depending on the relative volume fractions) surrounding nearly spherical inclusions of the minor phase [1]. The eutectic Bi–Sn is very different from both W–Cu and the steels, exhibiting a lamellar microstructure. Additionally, the CMCC model was previously applied only at very small strains for the steels (maximum of 0.6% total strain), and at very low strain rates for the Cu–W wires (the maximum strain rate where a composite was tested was $1 \times 10^{-7}\,\text{s}^{-1}$, above these strain rates only single phase Cu was tested) [1]. To the authors' knowledge this is the first time that this model is extended to large deformations and high creep rates (creep rates as high as $1 \times 10^{-2}\,\text{s}^{-1}$ over several seconds), as well as to a geometrically complex microstructure. While creep data for the Bi–42 wt % Sn eutectic has been previously published [2, 3], this is also the first time that the data and the constitutive equations for the Bi–10 wt % Sn solid solution and for the pure Bi phase are available.

2. Experimental procedure

The Sn–10 wt % Bi alloy was made from 99.99 wt % pure Sn and 99.9 wt % pure Bi. The pure Bi phase was also made from the 99.9 wt % pure Bi ingot. The Bi–42 wt % Sn eutectic, being 99.99 wt % pure, was provided by the Indium Corporation of America. All test samples were cast into test tubes. All Bi–42 wt % Sn samples were quenched into room temperature water, whereas Bi and Sn–10 wt % Bi samples were allowed to air-cool to room temperature. The castings were then machined into cylindrical dog-bone tensile bars, with a gauge diameter of 6.3 mm and a gauge length of 38 mm. All bars were then annealed for 12 h at 100 °C to relieve any residual stress that was possibly incurred by the machining. Some of the Bi–42 wt % Sn tensile bars were then aged in hot oil baths. Samples were tested in the as-quenched state,

after ageing for ten days at 120 °C, and after ageing for 22 days at 130 °C. Prior to testing, a facet was polished into the gauge section of several samples. This was done to observe the effect of the microstructural morphology on the amount of phase and grain boundary sliding. Creep tests performed under identical test conditions on unpolished samples showed that as long as the reduced cross-sectional area was taken into account, the facet did not effect the creep response. The Bi and Sn–10 wt % Bi tensile bars were tested in the as-cooled plus the 12 h anneal condition (consequently referred to as the as-cooled condition).

An Instron 4204 tensile tester with slotted grips was used for all testing. Strain in each sample was continuously monitored with an extensometer. The temperature of each test was controlled through the use of a box furnace surrounding the grip and sample assembly. Tests were performed at temperatures ranging from 20 to 120 °C with test temperatures varying no more than ± 3 °C.

Creep tests were conducted at constant applied load at low strain rates ($< 10^{-4}$ s^{-1}), and at a constant displacement rate at higher strain rates. For the low strain rate tests, a single sample was used at each temperature to collect data at various stresses. These tests were run only to steady-state creep, in general less than 0.1% strain, and in order of increasing load. For the constant displacement rate tests (where the samples underwent significant strain), a new sample was used at each stress. The strain rate reported corresponds to the strain rate at which the maximum stress was achieved.

3. Results

Fig. 2 shows the steady-state creep data of the Bi phase. The data show a power law behaviour and were fit with an empirical equation of the form

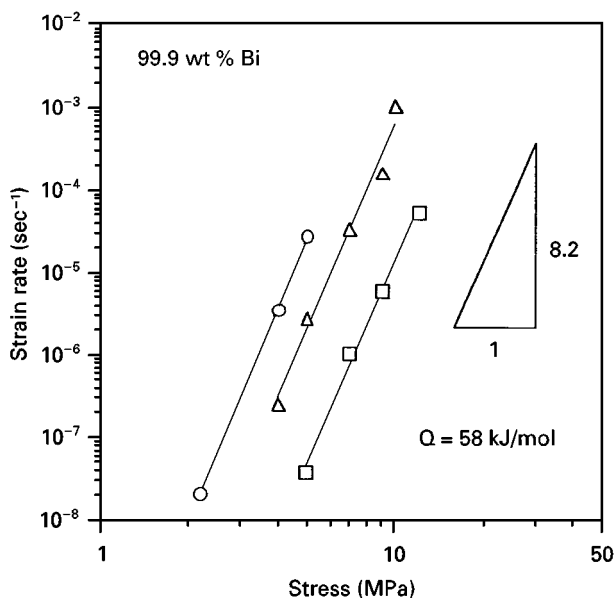$$\dot{\varepsilon}_{Bi} = \frac{CE}{kT}\left(\frac{\sigma}{E}\right)^n \exp\left(\frac{-Q}{kT}\right) \qquad (5)$$

where $\dot{\varepsilon}_{Bi}$ is the steady-state creep rate of Bi; σ is the applied stress; Q is the activation energy for Bi self-diffusion, 58 kJ mol^{-1} [24]; n is the stress exponent, 8.2; E is the Young's modulus, equal to $32.6 \times 10^3 - 46.8T$ MPa (where T is temperature in degrees celsius; the temperature dependence was determined in the course of the present study), and C is a creep constant equal to 10^{30} J mol^{-1} MPa^{-1} s^{-1} (obtained from the best fit of the data).

The Sn-rich data were fit using an empirical equation with a sinh stress dependence, because the data shows a combination power law (low-stress) and exponential (high-stress) stress dependence.

$$\dot{\varepsilon}_{Sn-10Bi} = \frac{CE}{kT}\left(\sinh\frac{\alpha\sigma}{E}\right)^n\left(\exp\frac{-Q}{kT}\right) \qquad (6)$$

where $\dot{\varepsilon}_{Sn-10Bi}$ is the steady-state creep rate of Sn–10 wt % Bi. The Young's modulus of the Sn-rich phase, as a function of temperature (°C), is $55\,580 - 8.31T - 1.14T^2$ MPa [25]. The constants C, α and n are 600 J mol^{-1} MPa^{-1} s^{-1}, 3000 and 1.8, respectively (obtained from best fit of the creep data). The Sn–10 wt % Bi alloy was tested only at 120 °C.

It is assumed that the creep rate of the Sn-rich phase is limited by the rate of diffusion of the Bi solute in the Sn matrix. This is a common observation for creep of binary solid solution alloys [6, 10]. Coarsening studies of the Bi–Sn eutectic [26] give a tracer diffusion activation energy of 73 KJ mol^{-1} for Bi in Sn. This activation energy is used in the present study as the creep activation energy in the Sn-rich phase.

Fig. 3 compares the steady-state data obtained from Bi–42 wt % Sn to that of the Bi phase and to Sn–10 wt % Bi, all tested at 120 °C. At stresses greater than 3 MPa, Sn–10 wt % Bi has a lower strain rate than pure Bi. Below 3 MPa, it appears that pure Bi is likely to have the lower strain rate, although the
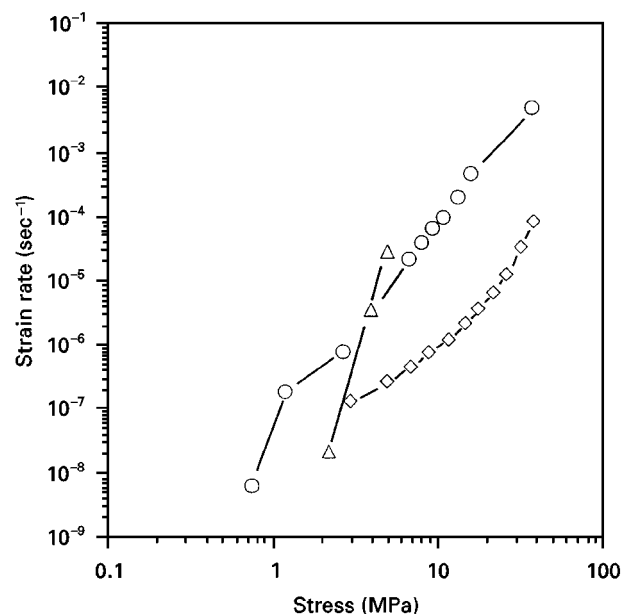
Figure 2 Steady-state creep rates of 99.9% Bi ($\square$ 20 °C, $\triangle$ 70 °C, $\bigcirc$ 120 °C).

Figure 3 Comparison of steady-state creep rates of 99.9% Bi, Sn–10 wt % Bi and Bi–42 wt % Sn at 393 K ($\diamond$ Sn–10Bi, $\triangle$ Bi, $\bigcirc$ Bi–42Sn).
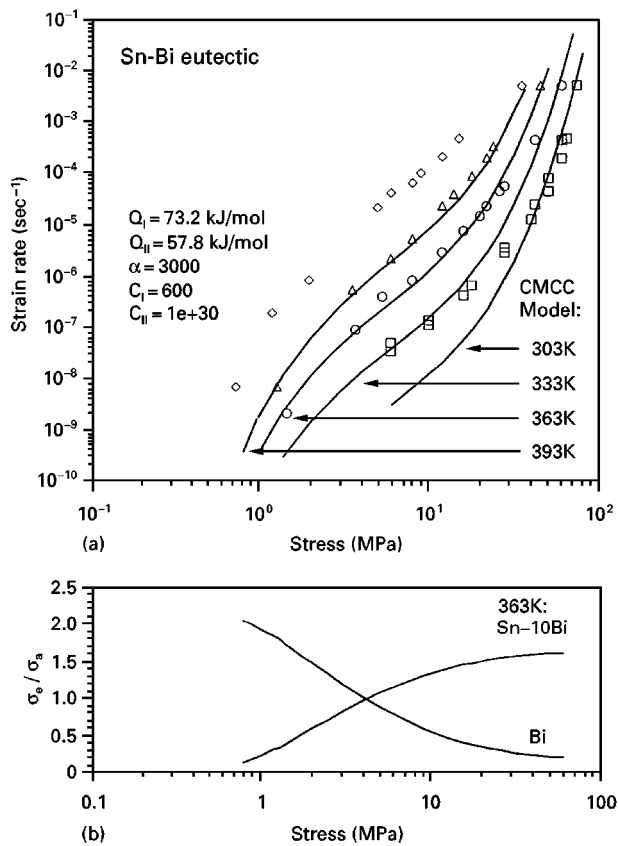
Figure 4 (a) Comparison of experimental and calculated creep rates of Bi–42 wt % Sn alloy at four temperatures and (b) normalized equivalent stress versus applied stress for each phase ($\square$ 303 K, $\bigcirc$ 333 K, $\triangle$ 363 K, $\diamond$ 393 K).

Sn–10 wt % Bi data do not extend to sufficiently low stresses to confirm this with absolute certainty. The creep rate of the composite is significantly faster than the creep rate of the individual phases.

Fig. 4a shows the Bi–42 wt % Sn eutectic steady-state creep data obtained from samples aged for ten days at 120 °C (as points) and the steady-state rates calculated from the CMCC model (as solid lines). The volume fraction of the Bi phase is 0.45. An intermediate value of 0.833 is used for the shape factor, K. Fig. 4b plots the normalized equivalent stress, σ_e^i/σ_{33}^A, for the individual phases of Bi–42 wt % Sn loaded at 90 °C, versus the applied stress, σ_{33}^A. It can now be seen that the equivalent stress in each of the load bearing phases (Bi at low stress, Sn–10 wt % Bi at high stress) is actually much higher than the applied stress.

The temperature dependence (spacing between the curves) and the stress dependence of the individual curves is in fair correlation to the experimental observations. However, the predicted creep rates are generally lower than the observed creep rates. It will be demonstrated that this may occur because there is a significant grain boundary sliding contribution to the overall creep rate in the eutectic.

4. Discussion

The Bi–42 wt % Sn steady-state data used to construct Fig. 4 were obtained from samples that were quenched

from the molten state and then aged for ten days at 120 °C. To determine the possible effects of microstructure on Bi–42 wt % Sn creep behaviour, creep tests were performed on two additional eutectic microstructures. Fig. 5a shows a backscattered electron micrograph of the as-quenched Bi–42 wt % Sn microstructure (light phase is Bi). Fig. 5b shows a backscattered electron micrograph of the quenched microstructure after aging for 22 days at 130 °C. It can be seen that significant coarsening and spheroidization of the eutectic microstructure is produced by aging. Whereas both phases are nearly continuous throughout the sample in the as-quenched state, the Bi phase becomes discontinuous in the aged condition. Similar results were also observed in a prior study on the ageing kinetics of Bi–Sn solder [27]. The microstructure of the samples used in Fig. 4 was of intermediate coarseness compared with these two extremes.

Fig. 6 shows the room temperature steady-state creep rates from these two sets of samples as well as the rates predicted by the CMCC model. Also shown are the creep rates reported for recrystallized Bi–42 wt % Sn [28]. The recrystallized samples had an equiaxed microstructure with a grain size of 6 μm [28]. Their creep rates are two to three orders of magnitude higher than the creep rates of the as-cast eutectic. Such an increase in the creep rate is typical of a material that begins to display significant grain
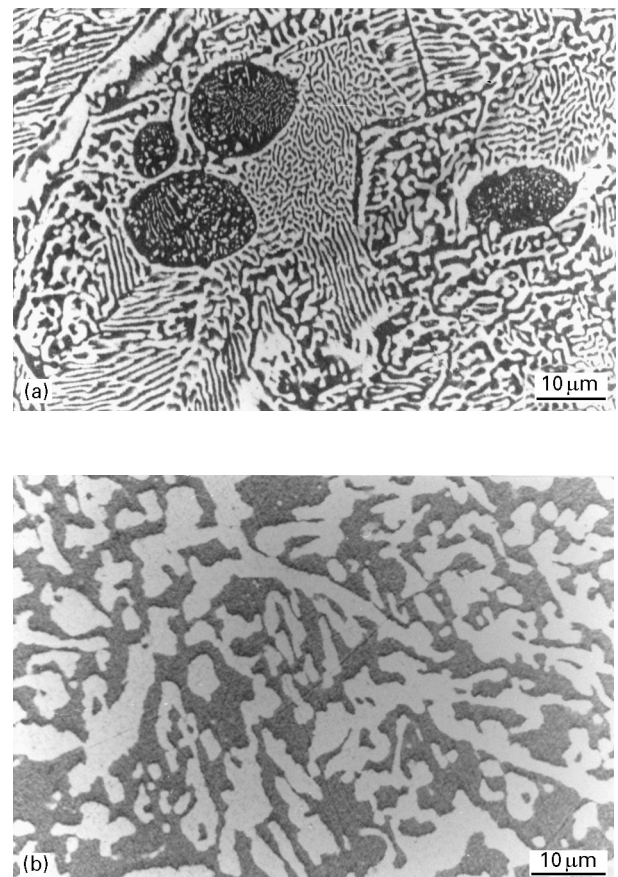

Figure 5 (a) Backscattered scanning electron micrograph of (a) the as-quenched Bi–42 wt % Sn microstructure and (b) the as-quenched Bi–42 wt % Sn microstructure after ageing for 22 days at 130 °C.
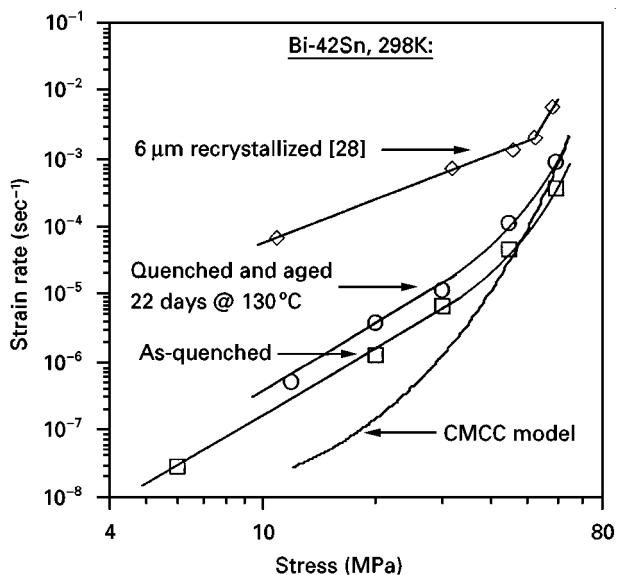
Figure 6 Steady-state creep rate of Bi–42 wt % Sn in the as-cast condition, aged 22 days at 130 °C, recrystallized, and CMCC model prediction at 298 K.

boundary or phase boundary sliding [29–31]. As the Bi–Sn eutectic microstructure becomes more and more spheroidized, the phases can slide past each other more freely. The increasing amount of phase boundary sliding should lead to increasing creep rates, as is observed.

In the Bi phase and in the Sn–10 wt % Bi, bulk creep mechanisms should dominate since both materials had an as-cast, single-phase microstructure where no phase boundary sliding could occur. Unfortunately, no microstructural data are available for the degree of grain boundary sliding in Sn–10 wt % Bi and in Bi. However, inferences about Sn–10 wt % Bi and about Bi can be made by observing the deformed Bi–Sn eutectic microstructure. Fig. 7a shows a backscattered electron micrograph of the deformed surface of a Bi–42 wt % Sn sample, that was aged for 22 days at 130 °C prior to testing. The sample was then strained 5% under an applied load of 20 MPa (strain rate of $5 \times 10^{-6}\,\mathrm{s}^{-1}$) at 20°C. Fig. 7b shows a topographical image of the same area. Phase boundaries in the coarser, spheroidized regions show more displacement than do boundaries in the finer, lamellar regions. There is significant displacement at the interface of the large Bi phase (in the middle of the micrograph) and the Sn phase that surround it. However, there is much less displacement between the grains within the Bi or the Sn rich phase (there is some grain boundary displacement within the Sn rich phase, and almost none within the Bi phase). This indicates that phase boundary sliding has a much larger contribution to the net deformation than does grain boundary sliding within the phase and implies that grain boundary sliding in the as-cast Sn–10 wt % Bi and Bi may be negligible compared to the bulk creep mechanisms. The conclusion that bulk creep mechanisms dominate deformation in the single-phase Sn–10 wt % Bi agrees with the results of Clark and Alden [31] who needed to cold work and anneal the single phase Sn–1 wt % Bi tensile specimens (resulting in equiaxed, recrystallized
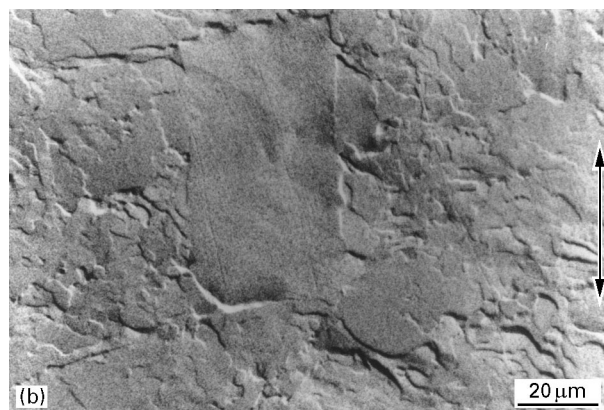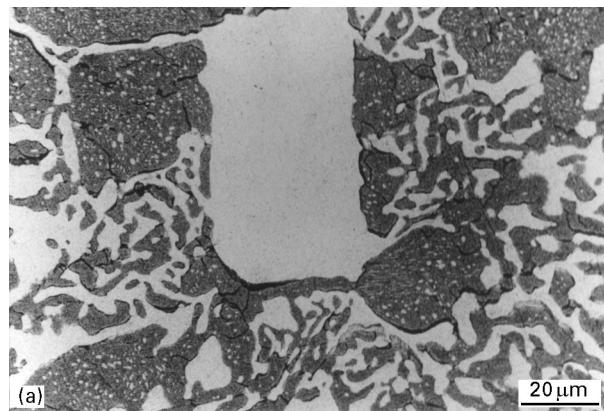

Figure 7 (a) Backscattered scanning electron micrograph of a deformed surface of Bi–42 wt % Sn that was aged for 22 days at 130 °C prior to testing (tested at 20 MPa, 20 °C). (b) Topographical image of the same area, showing phase and grain boundary displacements.

grains with a mean diameter of 2 µm) to obtain an appreciable amount of grain boundary sliding.

The major assumption in the CMCC model is that the phase and grain boundaries do not slide past each other. If the bulk creep mechanisms are accompanied by significant phase boundary sliding, the CMCC model will underestimate the data, as is observed in Fig. 6.

5. Conclusions

This study has demonstrated that the shape of the steady-state creep rate versus stress curve of the Bi–42 wt % Sn eutectic alloy is a result of the pure Bi phase being the load bearing phase at low stresses, and the Sn-rich phase being the load bearing phase at high stresses (> 3 MPa).

The continuum mechanics composite creep model is only partially effective in describing the deformation of the two-phase Bi–42 wt % Sn eutectic alloy because it assumes that continuity across the grains and phases is maintained. This assumption becomes invalid once significant phase boundary sliding occurs. Microstructural observations show that significant phase boundary sliding is present in the aged eutectic alloy, possibly explaining the order of magnitude discrepancy between predicted rates and the observed creep rates.

References

1. M. TANAKA, T. SAKAKI and H. IIZUKA, *Acta Metall.* **39** (1991) 1549.
2. G. D. SCHMEELK, Master Thesis, Rensselaer Polytechnic Institute (1993).
3. C. H. RAEDER, G. D. SCHMEELK, D. MITLIN, T. BARBIERI, W. YANG, L. E. FELTON, R. W. MESSLER, Jr, D. B. KNORR and D. LEE, in Proceedings of the 16th IEEE/CPMT IEMT Symposium, 12–14 September 1994, La Jolla, CA, p. l.
4. J. WEERTMAN, *J. Appl. Phys.* **28** (1957) 362.
5. *Idem, Trans. Met. Soc. AIME* **218** (1960) 207.
6. *Idem, J. Appl. Phys.* **28** (1957) 1185.
7. S. L. ROBINSON and O. D. SHERBY, *Acta Metall.* **17** (1969) 109.
8. J. WEERTMAN, in "Rate Processes in Plastic Deformation", edited by J. C. M. Li and A. K. Mukherjee (American Society for Metals, Metals Park, OH, 1975) p. 315.
9. T. G. LANGDON, in "Strength of Metals and Alloys", Proceedings of the 6th International Conference 1982, p. 1105.
10. P. YAVARI, F. A. MOHAMED and T. G. LANGDON, *Acta Metall.* **29** (1981) 1495.
11. D. L. McDANELS, R. A. SIGNORELLI and J. W. WEETON, ASTM STP 427 (American Society for Testing Materials, Philadelphia, PA, 1967) p. 124.
12. K. CHO and J. GURLAND, *Met. Trans.* **19** (1998) 2027.
13. M. H. POECH and H. F. FISCHMEISTER, *Acta Metall.* **40** (1992) 487.
14. K. S. RAVICHANDRAN, *ibid.* **42** (1994) 1113.
15. S. ANKEM and H. MARGOLIN, *Met. Trans.* **13A** (1982) 595.
16. K. TANAKA and T. MORI, *Acta Metall.* **18** (1970) 931.
17. K. TANAKA, K. WAKASHIMA and T. MORI, *J. Mech. Phys. Solids* **21** (1973) 207.
18. J. D. ESHELBY, *Proc. R. Soc.* **A241** (1957) 376.
19. *Idem, ibid.* **A252** (1959) 561.
20. T. MORI and K. TANAKA, *Acta Metall.* **21** (1973) 571.
21. T. MURA and T. MORI, *Micromechanics* **23** (1976).
22. T. MURA, "Micromechanics of Defects in Solids" (Martinus Nijhoff, The Hague, 1982).
23. K. TANAKA and T. MORI, *Acta Metall.* **18** (1970) 931.
24. W. P. ELLIS and N. H. NACHTRIEB, *J. Appl. Phys.* **10** (1969) 472.
25. B. M. DRAPKIN and V. K. KONONENKO, *Izvestia Akademii Nauk SSSR Metally* **2** (1987) 168.
26. E. L. HOLMES and W. C. WINEGARD, *Trans. Met. Soc. AIME* **224** (1962) 945.
27. C. H. RAEDER, D. MITLIN and W. YANG, in Proceedings of the Seventh International SAMPE Electronics Conference, Parsippany, NJ, 20–23 June, 1994, p. 355.
28. S. PATTANAIK and V. RAMAN, "Materials Developments in Microelectronics Packaging: Performance and Reliability", Conference Proceedings, edited by P. J. Singh (ASM International, 1991) p. 241.
29. D. H. AVERY and W. A. BACKOFEN, *Trans. ASM* **58** (1965) 551.
30. T. H. ALDEN, *J. Australian Inst. Metals* **14** (1969) 207.
31. M. A. CLARK and T. H. ALDEN, *Acta Metall.* **21** (1973) 1195.